Mercury Goes Solid At Room Temperature At Nanoscale: Toward An Effective Hg Waste Storage

N. Kana
University of South Africa
R. Morad
University of South Africa
M. Akbari
University of South Africa
M. Henini
Nottingham University
J. Niemela
International Centre for Theoretical Physics(ICTP)
F. Hacque
Rajshahi University
A. Gibaud
University of Le Maine
M. Maaza (Maaza@tlabs.ac.za)
University of South Africa

Research Article

Keywords: Quantum confinement, Solid mercury, Surface tension, phase transition, Laplace surface pressure

Posted Date: September 28th, 2021

DOI: https://doi.org/10.21203/rs.3.rs-917726/v1

Abstract

While room temperature bulk mercury is liquid, it is solid in its nanoconfiguration ($Ø_{nano-Hg} \leq 2.4$ nm). Conjugating the nanoscale size effect and the Laplace-driven surface excess pressure, Hg nanoparticles of $Ø_{nano-Hg} \leq 2.4$ nm embedded in a 2-D turbostratic BN host matrix exhibited net crystallization at room temperature via the experimentally observed (101) & (003) diffraction Bragg peaks of the solid Hg rhombohedric α-phase. The observed crystallization is correlated to a surface atomic ordering of 7 to 8 reticular atomic planes of the rhombohedric α-phase. Such a novel size effect on the phase transition phenomena in Hg is conjugated to a potential Hg waste storage technology. Considering the vapor pressure of bulk Hg, RT solid nano-Hg confinement represents a viable green approach for Hg waste storage derived from modern halogen-efficient light technology.

1. Introduction

Mercury is a unique metal that does not form diatomic molecules in the gas phase. Its bulk room temperature liquid property is correlated to its rare gas-like configuration (Xe) $^{6\ s24f14d10}$. More accurately, the relativistic contraction caused by the Dirac dynamics of the valence electrons (1). As a result of the relativistic mass increase $m = m_0/\sqrt{(1-(v/c))}$, "$v/c \sim 0.58$", the radial shrinkage of the effective Bohr radius $r_0 = (\varepsilon_0\ h/m_e\ e^2)$ of the inner "1 s" electrons is ~ 23%. Since the high-order "s" electronic shells have to be orthogonal against the lower shells, they will suffer a similar radius relativistic contraction, inducing a weak Coulomb interaction between neighboring Hg atomic sites.

Hg, as a singular liquid metal in its bulk form, has the highest elemental surface tension at room temperature, $\gamma \sim 486$ mN/m (2). The theoretical calculations on the liquid-vapor interface of simple metals in general (3–4) and methods based on the jellium model in particular (5), and the perturbation expansion up to the second order in the surface "e-ion" pseudopotential (6–7), showed that excessive surface tension could stimulate a significant surface atomic layering of 3–5 atomic planes, as depicted in Fig. 1.a & the corresponding periodic surface-to volume electron density profile. This surface atomic ordering, in full agreement with capillary wave theory, has been observed by X-ray reflectivity measurements on bulk liquid mercury surfaces by Pershan et al. (8). Likewise, Bafile et al (9–10) showed that such atomic ordering was able to be segregated in bulk liquid mercury by examining the height and width in addition to the position of the main peaks of the static structure factor S(Q) under ambient conditions. Both X-rays and neutron diffraction S(Q) profiles revealed a structure up to 4–5 discernable peaks: a feature of local surface atomic ordering (10).

Such an RT surface atomic ordering observed on the flat surface of bulk Hg could be enhanced significantly if not drastically on nano-Hg particles if one could engineer them. Indeed, as a result of their substantial surface/volume ratio and the 3-D symmetry breakdown, the surface atom population would be greater in nano-Hg. Henceforth, at such a scale, the surface phenomena dominate gravity effects in view of the significantly elevated surface tension of Hg (Fig. 1.b). The enhanced surface ratio of nano-Hg of radius "$Ø_{nano-}$Hg/2" should induce an excess of Laplace surface pressure $\Delta P \approx 4\gamma/Ø_{nano-Hg}$ of tens of

MPa. As an estimation, if $Ø_{nano-Hg} \approx 2.50$ nm, $\Delta P \approx 0.76$ GPa at RT. Considering the mercury phase diagram of Fig. 1.c, such an excess surface pressure at RT should induce net crystallization out of the liquidus space to the solid a-rhombohedric phase (11) of nano-Hg (Fig. 1.c). Hence, this atomic ordering phenomenon at RT should manifest itself through a significant crystallization of the liquid phase to the solid rhombohedral “α-type” phase.

2. Experiments, Experimental Results & Discussion

2. 1 Synthesis

For the first time, the synthesis of spatially isolated nano-Hg was demonstrated to be crystalline if its size was within the range of 2–5 nm. Such solidification was attributed to a size effect conjugated to the corresponding Laplace pressure excess. Apart from the safety aspect, the synthesis of nano-Hg was by itself an utmost challenge. The considered precursor was mercury(II) acetate $Hg(C_2H_3O_2)_2$. However, the foremost additional complexity remains in keeping the nano-Hg separated from each other; otherwise, the van der Waals/Otswald ripening type-induced agglomeration of the nano-Hg particles will generate larger Hg droplets and hence less surface pressure excess than the required threshold crystallization value of ≈ 0.76 GPa at RT. As schematically displayed in Fig. 1.d, a 2D boron nitride (BN)-isolated host matrix was used to prevent the coalescence process of nano-Hg. The deliberate choice of such a host matrix is its chemical inertness with Hg and its superior mechanical strength in addition to its 2-D structure.

The ideal precursors for obtaining the BN matrix were ortho-boric acid “H_3BO_3” and urea “H_2NCONH_2”, while mercury acetate “Hg $(C_2H_3O_2)_2$” was the optimal Hg precursor. The chemical reaction taking place was:

$$2H_3BO_3 + 1H_2NCONH_2 + \xi\ Hg\ (C_2H_3O_2)_2 \rightarrow \xi Hg + 2BN + \#\ Gases$$

While the initial H_3BO_3 and H_2NCONH_2 compositions were kept stoichiometric, the Hg $(C_2H_3O_2)_2$ was varied to obtain nano-Hg particles within the final BN host matrix. The relative molar initial concentration to the BN matrix of Hg $(C_2H_3O_2)_2$ was varied accordingly. The smaller this molar concentration is, the smaller the nano-Hg size. Different solutions of H_3BO_3, H_2NCONH_2 and $Hg(C_2H_3O_2)_2$ with molar fractions of 2,1 and ξ where “ξ” was varied from 1, 1/4 and 1/20 for Hg $(C_2H_3O_2)_2$ in deionized H_2O were prepared. The corresponding samples are labeled $Hg_{1/1}$-BN, $Hg_{1/4}$-BN, and $Hg_{1/20}$-BN.

2.2 Morphology & electron transmission studies

Figure 2.a reports a TEM of the $Hg_{1/20}$-BN nanocomposite. The voltage/exposure time was shortened drastically (≅ 20 secs) to minimize the agglomeration of nano-Hg. The observed rapid coalescence phenomenon was inherent to the insulating state of the nonpercolated Hg-BN nanocomposites and hence due to the lack of electronic charge and heat dissipation. Excluding the $Hg_{1/1}$-BN sample and freshly exposed to the incident electron beam, the Hg1/4–BN and $Hg_{1/20}$–BN nanocomposites consisted of

nanosized Hg isolated particles embedded in the BN host matrix. Their average diameter ⟨ $Ø_{nano-Hg}$ ⟩ at the early stage of electron beam exposure was estimated to be 3.83 and 2.41 nm in the $Hg_{1/4}$-BN and $Hg_{1/20}$-BN samples, respectively. $Hg_{1/1}$-BN consisted of relatively very large Hg particles within the submicron range. Subsequent to the heat generated by the TEM electron beam, the primarily well-dispersed nano-Hg began to coalesce promptly upon exposure to the electron microscopy beam even if the latter was kept at the minimum voltage possible. The TEM pattern of Fig. 2.a corresponds to the final morphological state of $Hg_{1/20}$-BN following an exposure duration of ∼14 s. Figure 2.b displays a slightly higher magnification ultrashort exposure time of the $Hg_{1/20}$-BN sample. If the Hg nanoparticles are almost quasi-spherical in shape with substantially truncated interfaces. The size polydispersity rose promptly subsequent to the slightly higher electron beam intensity. The new apparent diameter of the Hg nanoparticles ranges from 1.5 to 28.9 nm for the $Hg_{1/20}$-BN sample. Few larger distorted nano-Hgs of ∼63–70 nm in diameter are also observed. This could be congruent with sample zones that were exposed to noteworthy heat from the probing e-beam.

2.3-Crystallographic & phase transition investigations

Thereafter, the $Hg_{1/\xi}$-BN nanocomposites were investigated by XRD. A noteworthy consideration was assigned to the $Hg_{1/20}$-BN nanocomposite, as the TEM average size of the corresponding nano-Hg was $⟨Ø_{Hg}⟩_{TEM}$∼2.4 nm. These encaged nano-Hg particles are undersized sufficiently to undergo excess surface pressure above the threshold value of 0.76 GPa and hence would experience a diffraction feature.

Figure 3 displays the room temperature XRD profiles of $Hg_{1/1}$-BN (a), $Hg_{1/4}$-BN (b) and $Hg_{1/20}$-BN (c) and the liquid nitrogen (∼78 K) diffraction pattern of this latter (d), i.e., $Hg_{1/20}$-BN at ∼78 K. As shown in Fig. 3.a, excluding the (121) Bragg peak of the BN-t host matrix, the sample with the highest Hg concentration, i.e., $Hg_{1/1}$-BN does not exhibit any Bragg peak structure proper to mercury but rather a wide amorphous bump and a very broad peak extending over 10 Deg (40–50 Deg). These are signatures of an amorphous liquid without any long- or mid-range crystalline order.

Figure 3.b displays the diffraction pattern of the second lowest Hg concentration, i.e., $Hg_{1/4}$-BN. It exhibits 3 narrow diffraction peaks assigned to the BN-t host matrix (410), (132) and (203) Bragg peaks “ASTM Card 18–0251” (34). In addition, there is an intense but broad Bragg peak centered at 2Θ ∼ 32.719 Deg. This peak with a width at half maximum of ΔΘ ∼ 6.30 10^{-2} rad, can be assigned only to crystallized mercury, more precisely to the a-rhombohedric (101) reticular orientation “ASTM Card 09-0253” (35). Compared to the diffraction pattern of $Hg_{1/1}$-BN, yet broad, such a Bragg peak could be considered a signature of preliminary atomic ordering exhibited mostly by surface mercury atoms within the nonpercolated encaged nano-Hg. Using the Debye-Scherrer approximation for this Hg (101) Bragg peak, the average size of the corresponding Hg nanoparticles is ⟨ $Ø_{nano-Hg}$ ⟩ $_{DS}$ ∼ 2.43 nm. It is likely that such atomic-like ordering would originate from the surface atoms of the nano-Hg population and those with a smaller diameter according to the phase diagram of Fig. 1.c.

To conclusively corroborate the existence of this Hg (101) Bragg peak with surface atomic layering, the $Hg_{1/20}$-BN nanocomposite was examined extensively at both 293.5 (Fig. 3.c) and 78 K (Fig. 3.d). As it is the sample with the smallest mercury volume concentration, the corresponding nano-Hg with an average diameter of $\langle \emptyset_{nano-Hg} \rangle_{TEM}$ ~2.4 nm according to the TEM measurements would display the largest surface/volume ratio. The relative Hg (101) intensity should be superior for the same Hg volume concentration. As illustrated in Fig. 3.c, not only is the relative intensity of the Hg (101) Bragg peak is relatively larger for the $Hg_{1/20}$-BN nanocomposite but there is an additional Bragg peak centered at 2Θ ~ 39.695 Deg. Figure 4.a & its inset zooms explicitly (Fig. 4.b & Fig. 4.c) on this additional diffraction peak with a width at half maximum of ΔΘ ~ 3.580 Deg. Taking into account both its angular position and the relative intensity to the Hg (101) peak and the specific turbostratic structure of the host BN matrix (12), this Bragg peak could only be assigned to the 2nd intense crystalline Hg Bragg peak, i.e.. The Hg (003) crystallographic orientation of rhombohedric Hg α-phase “ASTM Card 09-0253”. To confirm that the indexed Hg (101) and Hg (003) are proper mercury Bragg peaks originating from the atomically ordered nano-Hg embedded in the BN-t host matrix, the sample Hg $_{1/20}$-BN was cooled to ~78.0 K. The labeled Hg (101) and Hg (003) develop sharper peaks with a significant angular shift, with 3 new less intense Hg Bragg peaks fitting with the Hg(110), Hg(104) and Hg(113) diffraction of solid a-rhombohedric solid Hg in addition to the presence of numerous $BN_{turbostatic}$ diffraction peaks (Fig. 4a & zoom inset). Therefore, the coexistence of the two Bragg peaks, namely, Hg(101) and Hg(003), in the room temperature diffraction pattern of the $Hg_{1/20}$-BN nanocomposite confirms the room temperature crystallization of the nonpercolated nano-Hg “$\langle \emptyset_{Hg} \rangle_{TEM}$ ~2.4 nm” within the BN-t host matrix. These experimental observations support a surface atomic layering consistent with even 7 to 8 atomic plane ordering (⟨a⟩~3.005 Å), as summarized in Fig. 4.d (13). Because of the vapor pressure of bulk Hg, embedding Hg in its nanoscale form in chemically inert BN matrices could be a significant advance in the safe storage of Hg and minimization of its hazardous aspect, especially Hg waste derived from modern halogen efficient light technology systems.

3. Conclusions

A size effect in nanoscale Hg dispersed in a 2-D BN host matrix was observed at room temperature. Hg nanoparticles with a diameter smaller than the threshold value of 2.5 nm, as defined by the P-T phase diagram, exhibit net crystallization manifesting itself through surface atomic layering of approximately 7–8 atomic layers. Below such a threshold value of 2.5 nm, Hg is solid at room temperature with an a-rhombohedric crystallographic structure with an average lattice parameter ⟨a⟩ ~ 3.005 Å. Considering the vapor pressure of liquid bulk Hg, embedding Hg in its nanoscale form in chemically inert BN matrices could be of a significant advance in the safe storage of Hg and minimization of its hazardous aspect, especially Hg waste derived from modern halogen-efficient light systems.

Declarations

Acknowledgment

The authors wish to extend their gratitude to the various funding agencies & institutions that supported this research project, including the UNESCO UNISA ITL-NRF Africa Chair in Nanosciences & Nanotechnology (U 2ACN2), The University of South Africa (UNISA), iThemba LABS, the National Research Foundation of South Africa (NRF), and the French Centre National pour la Recherche Scientifique (CNRS). One of us (MM) wishes to dedicate this contribution to Prof. M.O. Osman Ndwandwe & Prof. F. R. L. Schoening & Mrs. J.Salemi.

References

1. Pyykkö, P.," Relativistic Effects in Structural Chemistry" *Adv. Quantum Chem*.11, p.353 (1978).
2. Wilkinson, M.C.,"" *Chem. Rev.*72, N°6, p.575 (1972).
3. Evans, R., " The Monte Carlo method for the study of phase transitions: A review of some recent progress" *J. Phys.* C.7, p.2808 (1974).
4. Amokrane, S. et al," A pseudoatom theory for the liquid–vapor interface of simple metals" *J. Phys. Chem*.75, p.5543 (1982).
5. Lang, N.D., et al, "Theory of Metal Surfaces" *Phys. Rev. B.*12, p.4555 (1970).
6. Chacon, E. et al, " Nonlocal kinetic energy functional for nonhomogeneous electron systems" *Phys. Rev.B*.32, p.7868 (1985).
7. Gomez, M. A. et al, " Electronic structure: wide-band, narrow-band, and strongly correlated systems, Phys. Rev. B 46, 6665 (1992)
8. Magnussen, M. et al, " X-ray Reflectivity Measurements of Surface Layering in Liquid Mercury" *Phys. Rev. Lett.*74, N°22, p.4444 (1995).
9. Bafile, U. et al, " Ab initio molecular dynamics study of the static, dynamic, and electronic properties of liquid mercury at room temperature "*J. Non-Cryst. Solids.* 250-252, p.35 (1999).
10. U. Bafile, et al, " The microscopic structure of liquid mercury from neutron and X-ray diffraction" *Physica. B.*276-278, p.452 (2000).
11. Young, B., in" Phase Diagram of Elements", University of California Publishing (1992).
12. Matsui, T. et al, " Synthesis and characterization of cerium oxide nanoparticles coated with turbostratic boron nitride" *J. Mater. Chem.*, 2003, 13, 622–627 (2003).
13. Gaston, N. et al, " The lattice structure of mercury: Influence of electronic correlation" *Phys. Rev.B,* 1098-0121,(2006).

Figures

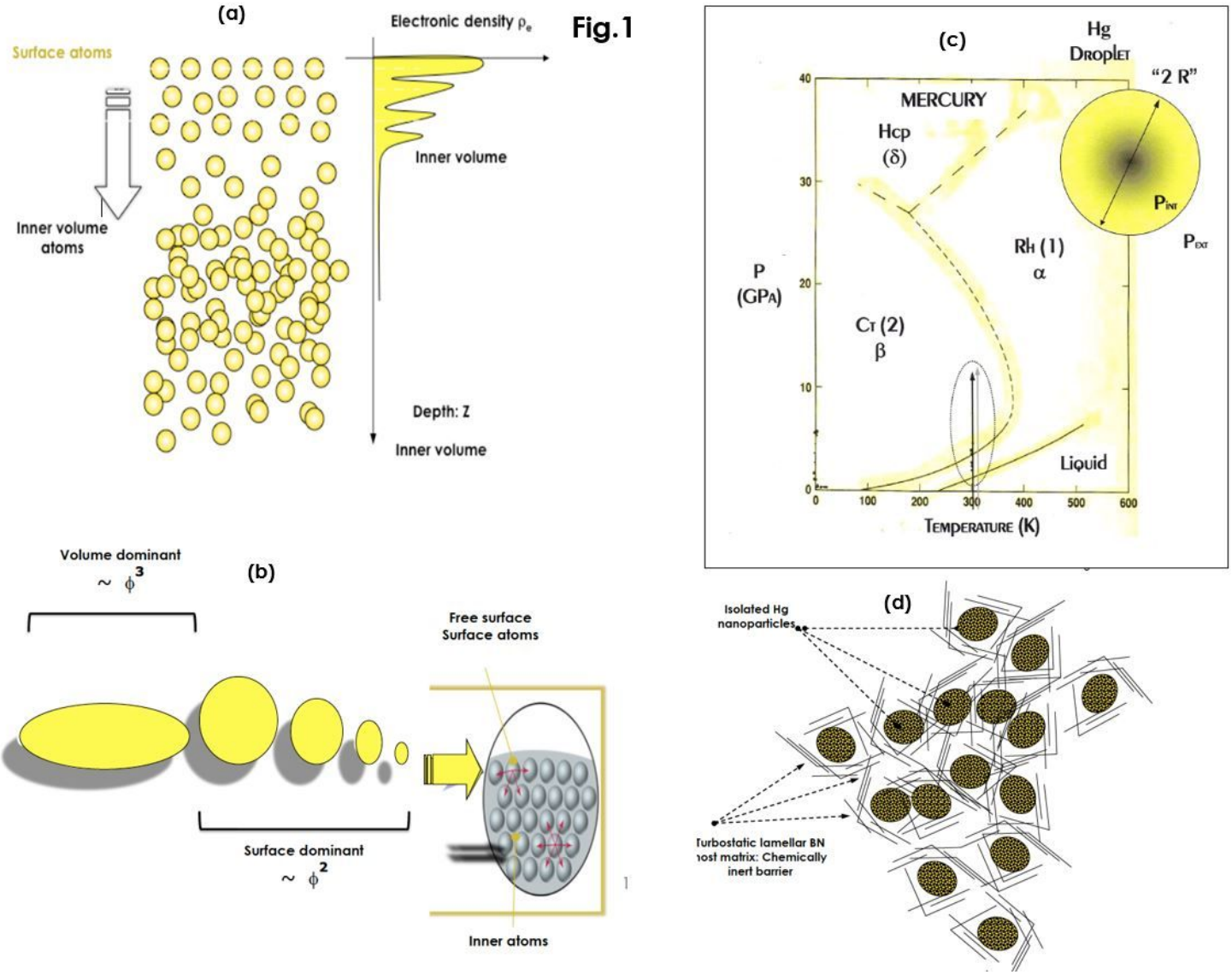

Figure 1

(a) Theoretical surface atomic ordering in liquid Hg with the corresponding in depth variation of the electronic density, (b) Schematic representation of volume & surface driven shape anisotropy in Hg droplets, c) Hg phase diagram (according to [11]), (d) Schematic representation of the Hg nanoparticles confined in turbostratic BN chemically inert host matrix.

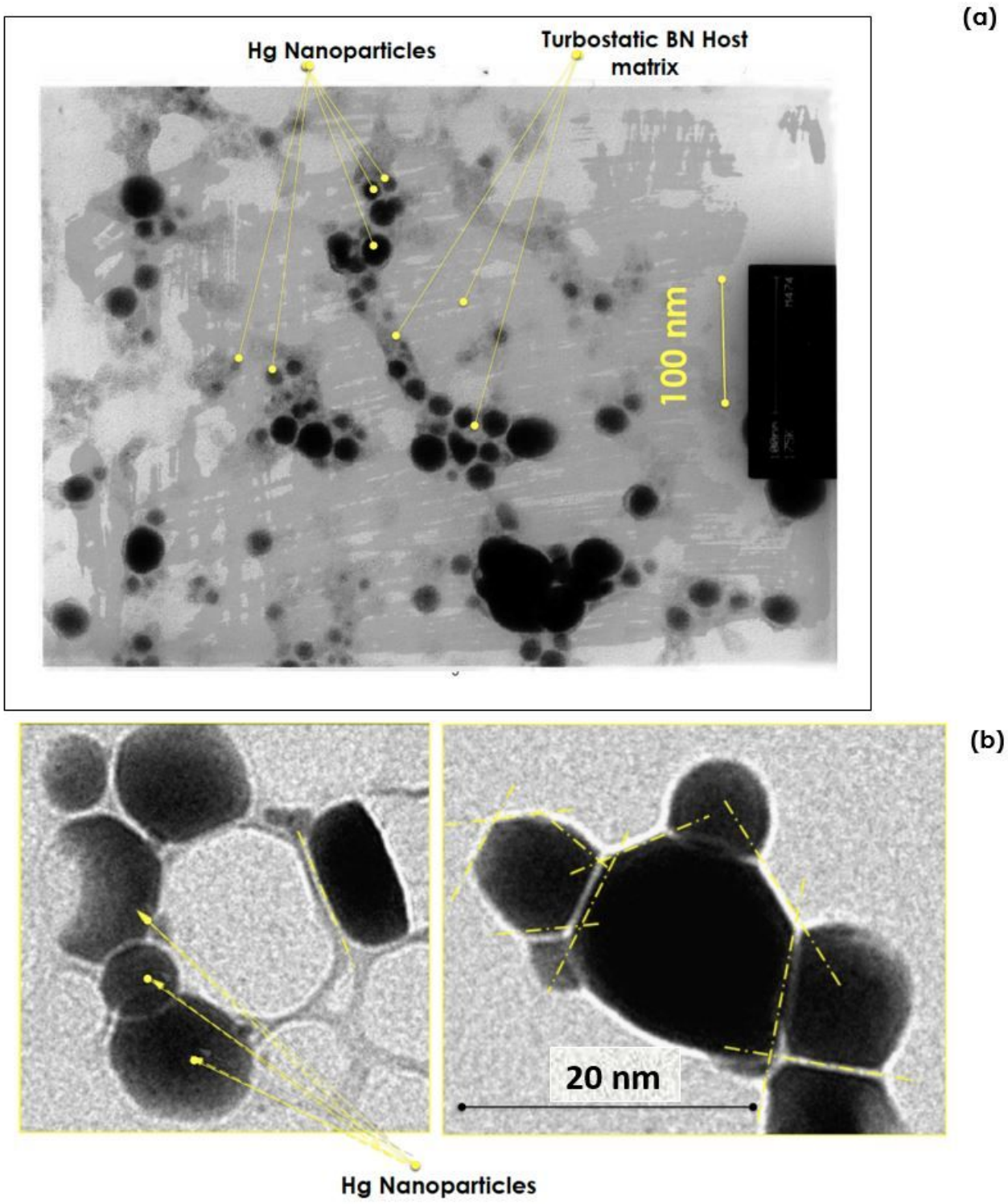

Figure 2

(a) Low- and (b) High-magnification transmission electron microscopy of the Hg1/20-BN nanocomposite with an early-stage average size of the Hg nanoparticles (ØHg)TEM ~2.4 nm dispersed in the turbostratic BN matrix of the Hg1/20-BN nanocomposite

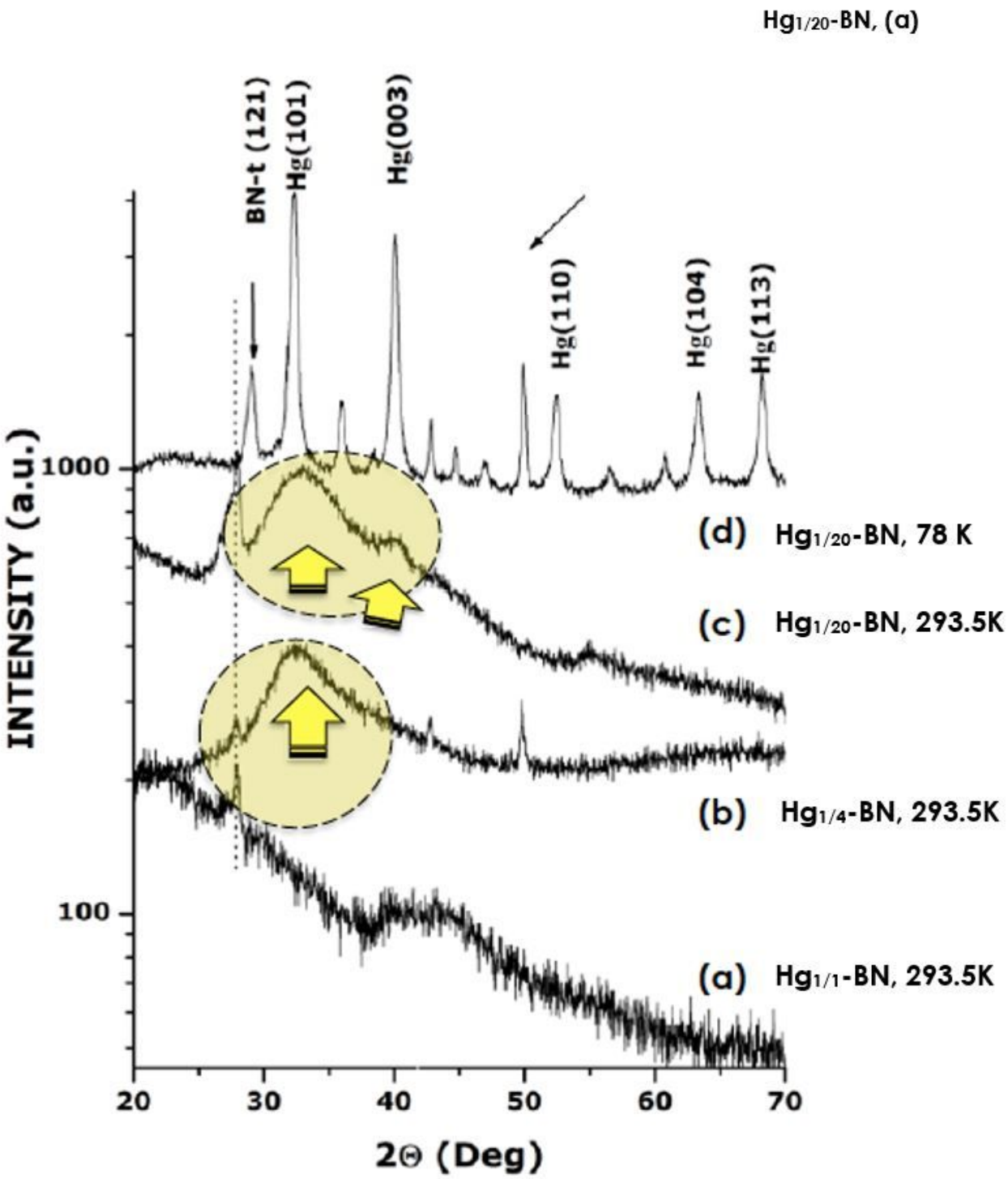

Figure 3

Room temperature X-ray diffraction profiles of the 3 different samples: (a) Hg1/1-BN, (b) Hg1/4-BN, (c) Hg1/20-BN and (d) nitrogen temperature diffraction pattern of the latter sample “Hg1/20-BN nanocomposite at ~78 K.

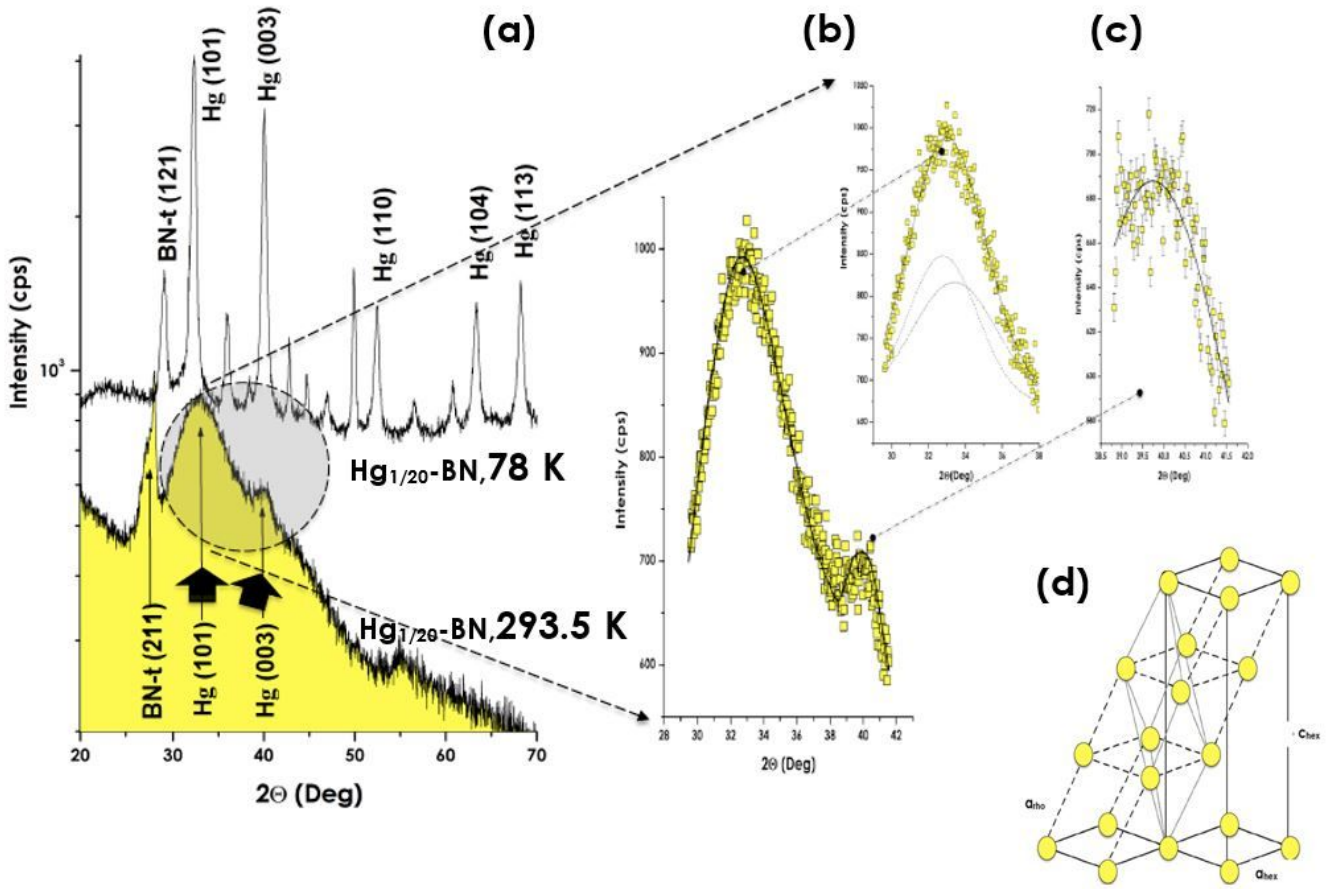

Figure 4

(a) Room temperature X-ray diffraction profiles of Hg1/20-BN and its nitrogen temperature. The inset (b,c) displays a magnification of the (101) & (003) Bragg peak inferred to (d) solid α-rhombohedric atomic ordering of encaged nanoscale Hg with 7-8 ordered atomic layers.

Supplementary Files

This is a list of supplementary files associated with this preprint. Click to download.

- ADINFORMATIONSOLIDMERCURYVR10.docx